Fast High-Order Terminal Sliding-Mode Current Controller for Disturbance Compensation and Rapid Convergence in Induction Motor Drives

Tianqing Wang, Bo Wang, *Member, IEEE*, Yong Yu, and Dianguo Xu, *Fellow, IEEE*

***Abstract*—By ensuring the finite-time convergence to equilibrium point under disturbance, the high-order terminal sliding-mode (HO-TSM) current controller can improve the system robustness for induction motor (IM) drives. However, the existing HO-TSM still suffers from the drawback that it cannot obtain rapid convergence and effective chattering suppression simultaneously. To address this problem, a fast HO-TSM current controller is studied with the modifications from three aspects. First, a fast HO-TSM surface is designed to improve the convergence speed when the system state is ON the designed surface. Second, the control law is modified with a linear integral term to enhance the capability of disturbance compensation. Third, a nonlinear gain is introduced to adjust the gain value, leading to satisfactory chattering suppression during steady state. Compared with conventional HO-TSM, the studied method can achieve strong robustness to disturbance, rapid convergence, and improved chattering suppression capability at the same time. Finally, the superiority of studied method is verified by the experimental results from a 3.7 kW IM test bench.**

***Index Terms*—Anti-disturbance capability, current loop, high-order terminal sliding-mode (HO-TSM), induction motor (IM) drives.**

I. Introduction

AS THE key factor of overall induction motor (IM) driving performance, the current controller has been constantly improved over the past decade to adapt the high-end IM applications with harsh working condition [1], [2], e.g., high-speed locomotive traction system, and aircraft steering motor control system. Under such working condition, the current controller is expected to achieve rapid dynamic under various system disturbances, such as the variations of load torque and motor operation condition, cross-coupling terms, and uncertainty of IM parameters [2], [3]. For the classic proportional–integral (PI) current controller, by achieving pole-zero cancellation with PI gains, the current control performance can be regulated by its control bandwidth [4]. However, there are two factors that will degrade the performance of PI control.

First, the limitation of control bandwidth. To ensure the control accuracy at steady state, the control bandwidth needs to be limited [5], and this factor is common in the cost-critical IM applications with relatively low carrier frequency.

Second, the variation of IM parameters. The effectiveness of pole-zero cancellation is on the basis of accurate IM parameters. However, in the actual application when the motor requires to work for a long time and usually copes with rapid reference speed and load torque changes (e.g., motors for crane, winch), the motor parameters will change inevitably due to the operation conditions and temperature, resulting in the degradation of PI control performance [4].

To achieve the desirable current control performance, much endeavor has been made to replace the conventional PI control with other control methods. It includes the methods to increase the convergence speed (e.g., various predictive control strategies [6]); the methods to improve the robustness to disturbance (e.g., different types of disturbance observer-based control [4], [7]), and the combination of the above two categories [8]. In addition to the above methods, the sliding-mode control (SMC) has also attracted many research interests because of its unique virtues of the following two respects.

1) The capability to adjust the system convergence trajectory. In SMC strategy, the convergence process usually contains two stages: the approaching stage and the sliding stage [9]. The system will go through these two stages in sequence until reaching the equilibrium point [10]. Thus, the system convergence process can be regulated by the design of SMC law and sliding-mode surface.
2) High robustness to system parameters due to the invariant properties to disturbance [11]. In SMC strategy, the equivalent control term, which uses the known system dynamic, usually requires the system parameters [9], [10], [11], [12]. Here, the system parameters variation is inevitable, but can be deemed as disturbance. Then, by selecting the control gain above the boundary of disturbance, the control law can ensure the convergence to equilibrium point, leading to the improved robustness to system parameters [13].

Although these advantages of SMC are tempting for motor drives system, the corresponding problems still need to be addressed.

Manuscript received 16 January 2023; revised 12 April 2023; accepted 16 May 2023. Date of publication 19 May 2023; date of current version 21 June 2023. This work was supported in part by the National Natural Science Foundation of China under Grant 52177030. Recommended for publication by Associate Editor K. Basu. *(Corresponding authors: Bo Wang; Yong Yu.)*

The authors are with the School of Electrical Engineering and Automation, Harbin Institute of Technology, Harbin 150001, China (e-mail: 19S006067@stu.hit.edu.cn; wangbohit@hit.edu.cn; yuyong@hit.edu.cn; xudiang@hit.edu.cn).

Color versions of one or more figures in this article are available at https://doi.org/10.1109/TPEL.2023.3277886.

Digital Object Identifier 10.1109/TPEL.2023.3277886

First, the motor current loop is a first-order system. The conventional sliding-mode surface, i.e., current error itself, cannot represent any convergence dynamics, resulting in the disappearance of sliding stage [14]. To address this problem, some nonsingular terminal sliding-mode surfaces are proposed for first-order system [15], [16]. However, these sliding-mode surface contain fractional powers terms of system variable derivative, which bring difficulties for implementation. In [17], integral sliding-mode surfaces are studied to introduce the designed convergence trajectories, but the system still cannot achieve high-order sliding-mode dynamic.

Second, the conventional SMC aims to achieve the convergence of sliding-mode variable to zero, and its high robustness requires high gains of switching control. Then, the discontinuous control law acts directly on the derivative of sliding mode variable, resulting in the well-known chattering problem [18]. Some existing solutions use the saturation or power function to replace the switching function. It can reduce the chattering but also break the Lyapunov stability of SMC [19].

High-order SMC law is an effective approach to address the above problems. Compared with the previous SMC, the high-order SMC aims to achieve the convergence of both sliding-mode variable and its derivative to zero [20]. Here, the switching control is hidden in the derivative of control law, so that the control law becomes a continuous function, leading to chattering suppression. Meanwhile, by ensuring the control gain value is higher than the boundary of the disturbance derivative, the stability of high-order SMC can be guaranteed so that the high robustness to disturbance can be preserved [2]. In [21] and [22], a typical high-order SMC called supertwisting algorithm (STA) is adopted for current controller design to achieve static-errorless control and chattering suppression. However, the super-twisting has the problem that its control performance is sensitive to system disturbance [2].

Except for the above methods, the high-order terminal sliding-mode (HO-TSM) is also a promising solution to address the problems of conventional SMC. The HO-TSM aims to achieve the finite-time convergence to terminal sliding-mode surface, and then achieve the convergence of both sliding-mode variable and its derivative to zero [23]. Thus, compared with conventional terminal SMC, it has the advantages of full-order sliding-mode dynamics, avoiding the singularity problem, and chattering suppression capability. Due to these advantages, the HO-TSM has been implemented in motor drives system as speed controller [24] and rotor flux estimator [25]. In the current controller, the system dynamic should be much faster than the speed controller or flux estimator. However, the only solution for the existing HO-TSM to achieve fast dynamic response under disturbance is to select high value control gains. In digital control system, the high value gains of unsmooth control term will result in the aggravation of chattering problem.

To address this problem, a fast HO-TSM is proposed for IM current controller. The innovation of the studied method consists of three aspects.

1) The sliding-mode surface of the conventional HO-TSM is modified by a smooth control term to increase the convergence speed.
2) Based on the designed surface, the control law is augmented by a linear integral control term to increase the speed of disturbance compensation.
3) A nonlinear gain is introduced to adjust gain value for chattering suppression.

Compared with conventional HO-TSM, the proposed current controller can possess strong robustness to system disturbance, rapid convergence, and desirable chattering suppression capability simultaneously. Finally, the comparative experimental results are provided to verify the studied method.

II. Modeling and System Description

A. Modeling of IM

In synchronous rotating d–q reference frame, the mathematical model of IM can be described as [1]

$$\begin{cases} \frac{di_{sd}}{dt} = -\frac{R_s L_r^2 + R_r L_m^2}{\sigma L_s L_r^2} i_{sd} + \omega_e i_{sq} + \frac{L_m}{\sigma L_s L_r T_r} \lambda_r + \frac{u_{sd}}{\sigma L_s} \\ \frac{di_{sq}}{dt} = -\frac{R_s L_r^2 + R_r L_m^2}{\sigma L_s L_r^2} i_{sq} - \omega_e i_{sd} - \frac{L_m}{\sigma L_s L_r} \omega_r \lambda_r + \frac{u_{sq}}{\sigma L_s} \end{cases} \tag{1}$$

where i_{sd} and i_{sq} are stator current d–q components; u_{sd} and u_{sq} are stator voltage d-q components; R_s and R_r are stator and rotor resistances; L_s, L_r, and L_m are self and mutual inductances; λ_r is rotor flux; ω_e is synchronous angular speed; ω_r is rotor angular speed; $T_r = L_r / R_r$ is rotor time constant; and $\sigma = 1 - L^2{}_m / (L_s L_r)$ is leakage coefficient.

For clarity, the matrix form of (1) can be written as

$$\frac{d\boldsymbol{i}}{dt} = \boldsymbol{A}\boldsymbol{i} + \boldsymbol{B} + \boldsymbol{C}\boldsymbol{u} \tag{2}$$

where $\boldsymbol{i} = \begin{bmatrix} i_{sd} & i_{sq} \end{bmatrix}^T$; $\boldsymbol{u} = \begin{bmatrix} u_{sd} & u_{sq} \end{bmatrix}^T$; $\boldsymbol{A} = -a\boldsymbol{I} - \omega_e \boldsymbol{J}$; $\boldsymbol{B} = \begin{bmatrix} \frac{L_m \lambda_r}{\sigma L_s L_r T_r} & -\frac{L_m \lambda_r}{\sigma L_s L_r} \omega_r \end{bmatrix}^T$; $\boldsymbol{C} = \frac{1}{\sigma L_s} \boldsymbol{I}$; $a = \frac{R_s L_r^2 + R_r L_m^2}{\sigma L_s L_r^2}$; $\boldsymbol{I} = \begin{bmatrix} 1 & 0 \\ 0 & 1 \end{bmatrix}$; and $\boldsymbol{J} = \begin{bmatrix} 0 & -1 \\ 1 & 0 \end{bmatrix}$.

The IM model (2) is written under ideal conditions. However, the IM model is inevitably affected by system disturbances, including two aspects: the IM parameters uncertainty and variation and external disturbance from the outer loop and other unmodeled dynamics [2], [3]. Thus, the system disturbance should be included. Defining the current tracking error $\boldsymbol{e}$ as

$$\boldsymbol{e} = \boldsymbol{i} - \boldsymbol{i}_{\text{ref}} = \begin{bmatrix} e_{sd} & e_{sq} \end{bmatrix}^T \tag{3}$$

where $\boldsymbol{i}_{\text{ref}}$ is the current reference value $\boldsymbol{i}_{\text{ref}} = [i_{sd,\text{ref}}\ i_{sq,\text{ref}}]^T$.

Then, the dynamic equation of the current tracking error with system disturbance can be described as

$$\begin{aligned} \frac{d\boldsymbol{e}}{dt} &= (\boldsymbol{A} + \Delta\boldsymbol{A})\,\boldsymbol{i} + (\boldsymbol{B} + \Delta\boldsymbol{B}) + (\boldsymbol{C} + \Delta\boldsymbol{C})\,(\boldsymbol{u} + \varepsilon) - \frac{d\boldsymbol{i}_{\text{ref}}}{dt} \\ &= \boldsymbol{A}\boldsymbol{i} + \boldsymbol{B} + \boldsymbol{C}\,(\boldsymbol{u} + \boldsymbol{d}) \end{aligned} \tag{4}$$

where, $\Delta[\cdot]$ represents the uncertainty and variation of IM parameters; ε represents the unmodeled dynamics; and $\boldsymbol{d} = \begin{bmatrix} d_{sd} & d_{sq} \end{bmatrix}^T$ is defined as the lumped disturbance:

$$\boldsymbol{d} = \boldsymbol{C}^{-1} \left(\Delta\boldsymbol{A}\boldsymbol{i} + \Delta\boldsymbol{B} + \Delta\boldsymbol{C}\,(\boldsymbol{u} + \varepsilon) - \frac{d\boldsymbol{i}_{\text{ref}}}{dt} \right) + \boldsymbol{\varepsilon}. \tag{5}$$

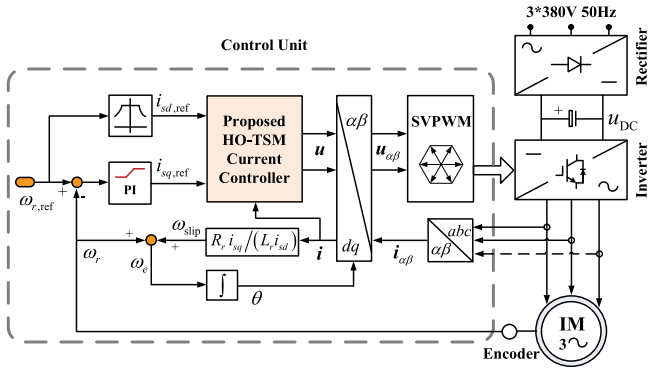

Fig. 1. Block diagram of the IM drive with proposed current controller.

Then, for the actual IM application, the system disturbance $\boldsymbol{d}$ is analyzed by following two conditions.

1) During the steady state, the stator current ($\boldsymbol{i}$, and $\boldsymbol{i}_{\mathrm{ref}}$), operation speed ($\omega_e$, and ω_r), and rotor flux λ_r can all be considered as constant value. The variation speed of IM parameters is slow. Thus, in the steady state, the $\boldsymbol{d}$ can be considered as a constant value disturbance [3]

$$\left\|\dot{\boldsymbol{d}}\right\| = \max\left(\left|d_{sd}\right|, \left|d_{sq}\right|\right) = 0. \tag{6}$$

2) During the transient state, the stator current, operation speed, and rotor flux are all variation states changing with time and IM operation condition. Thus, in the transient state, the $\boldsymbol{d}$ can be considering a variation disturbance

$$0 < \left\|\dot{\boldsymbol{d}}\right\| < \eta \tag{7}$$

where η is a positive constant represents the boundary of the system disturbance derivative.

B. System Description of IM Drives

Fig. 1 shows the block diagram of the field-oriented control (FOC) based IM drive. The cascade double closed-loop structure is adopted as the basic control strategy. The outer loop is the speed loop with PI control. The inner loop is the current loop using the proposed HO-TSM controller. The input of the current controller $i_{sd,\mathrm{ref}}$ (field current) is a constant value within the rated speed; and the $i_{sq,\mathrm{ref}}$ (torque current) varies according to the speed controller output. The output of the current controller $\boldsymbol{u}$ is designed to achieve satisfactory current control performance under the influence of system disturbance.

III. HO-TSM Current Controller

As the inner loop of IM system, the designed sliding-mode current controller is expected to possess three characteristics.

1) Strong robustness to system disturbance.
2) Rapid convergence capability.
3) Chattering suppression capability.

In the rest of this section, the conventional HO-TSM current controller is first introduced. Then, the controller is evaluated by the above three characteristics to reveal the advantages and disadvantages of the HO-TSM.

A. HO-TSM Current Controller

For the first-order system in (4), the current tracking error $\boldsymbol{e}$ is selected as the variable of the sliding-mode controller. Then, the HO-TSM surface is designed as [22]

$$\boldsymbol{s} = \frac{d\boldsymbol{e}}{dt} + \alpha|\boldsymbol{e}|^p \mathrm{sgn}\left(\boldsymbol{e}\right) \tag{8}$$

where $\mathrm{sgn}(\mathbf{e}) = \left[\mathrm{sgn}(e_{sd}) \quad \mathrm{sgn}(e_{sq})\right]^T$; $|\boldsymbol{e}|^p$is defined as the diagonal matrix $|\boldsymbol{e}|^p = \mathrm{diag}(|e_{sd}|^p, |e_{sq}|^p)$, $0< p < 1$, and $\alpha > 0$ is the control gain of the sliding-mode surface.

The HO-TSM surface introduces the ideal convergence dynamic $\boldsymbol{s} = 0$ when the system is not affected by disturbance. By substituting $\boldsymbol{s} = 0$ into (8), it yields

$$d\boldsymbol{e}/dt = -\alpha|\boldsymbol{e}|^p \mathrm{sgn}\left(\boldsymbol{e}\right). \tag{9}$$

From (9), in the undisturbed system, the current error can converge to equilibrium point $d\boldsymbol{e}/dt = \boldsymbol{e} = 0$ within finite-time t_1

$$t_1 = \left\|\boldsymbol{e}\left(0\right)\right\|^{1-p} \Big/ \alpha\left(1-p\right). \tag{10}$$

To achieve the convergence dynamic of (9), the control law of the HO-TSM current controller is designed as $\boldsymbol{u} = \boldsymbol{u}_{eq} + \boldsymbol{u}_n$

$$\begin{cases} \boldsymbol{u}_{eq} = -\boldsymbol{C}^{-1}\left(\boldsymbol{A}\boldsymbol{i} + \boldsymbol{B} + \alpha|\boldsymbol{e}|^p \mathrm{sgn}\left(\boldsymbol{e}\right)\right) \\ \dot{\boldsymbol{u}}_n = -k_1 \mathrm{sgn}\left(\boldsymbol{s}\right) \end{cases} \tag{11}$$

where $\boldsymbol{u}_{eq}$ represents the equivalent control term; $\boldsymbol{u}_n$ is the integral control law with initial condition $\boldsymbol{u}_n(0) = 0$; and k_1 is the designed integral control gain. By substituting (11) into (4), the convergence dynamic of the HO-TSM is

$$d\boldsymbol{e}/dt = -\alpha|\boldsymbol{e}|^p \mathrm{sgn}\left(\boldsymbol{e}\right) + \boldsymbol{C}\left(\boldsymbol{d} - \int k_1 \mathrm{sgn}\left(\boldsymbol{s}\right) dt\right). \tag{12}$$

In the undisturbed system without $\boldsymbol{d}$, ideal dynamic $\boldsymbol{s} = 0$ can be achieved only by the $\boldsymbol{u}_{eq}$. However, the system disturbance is inevitable in the actual control system. Thus, the HO-TSM must contain the disturbance-compensate term $\boldsymbol{u}_n$ to force the system back to the ideal convergence dynamic.

Theorem 1: If the selected integral control gain satisfies the following condition:

$$k_1 > \eta > \left\|\dot{\boldsymbol{d}}\right\| \tag{13}$$

the control law in (11) can compensate the system disturbance $\boldsymbol{d}$ (with initial condition $\boldsymbol{d}(0)$) in a finite-time t_2

$$t_2 \le \left\|\boldsymbol{d}\left(0\right)\right\| / \left(k_1 - \eta\right). \tag{14}$$

Proof: By substituting (4) into (8), the HO-TSM surface can be rewritten as

$$\boldsymbol{s} = \boldsymbol{A}\boldsymbol{i} + \boldsymbol{B} + \boldsymbol{C}\left(\boldsymbol{u} + \boldsymbol{d}\right) + \alpha|\boldsymbol{e}|^p \mathrm{sgn}\left(\boldsymbol{e}\right). \tag{15}$$

Substituting the control law (11) into (15), we can obtain

$$\boldsymbol{s} = \boldsymbol{C}\left(\boldsymbol{u}_n + \boldsymbol{d}\right). \tag{16}$$

Then, the derivative of (16) with respect to time is

$$\dot{\boldsymbol{s}} = \boldsymbol{C}\left(\dot{\boldsymbol{d}} - k_1 \mathrm{sgn}\left(\boldsymbol{s}\right)\right) \le \boldsymbol{C}\left(\eta - k_1 \mathrm{sgn}\left(\boldsymbol{s}\right)\right). \tag{17}$$

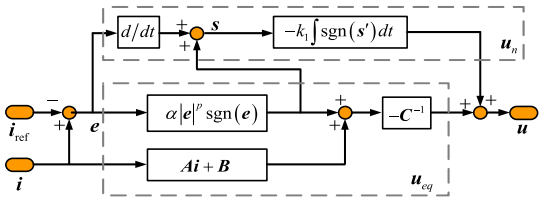

Fig. 2. Block diagram of the conventional HO-TSM current controller.

According to (16), the initial value of $\boldsymbol{s}$ can be expressed as: $\boldsymbol{s}(0) = \boldsymbol{C}(\boldsymbol{u}_n(0) + \boldsymbol{d}(0)) = \boldsymbol{C}\boldsymbol{d}(0)$. Considering a Lyapunov function: $V = 0.5\boldsymbol{s}^T\boldsymbol{s}$. Then, the derivative of V with respect to time is $\dot{V} = \boldsymbol{s}^T\dot{\boldsymbol{s}}$. From (17), $\dot{V}$ can be rewritten as follows:

$$\boldsymbol{s}^T\dot{\boldsymbol{s}} = \boldsymbol{C}\left(\boldsymbol{s}^T\dot{\boldsymbol{d}} - k_1\boldsymbol{s}^T\mathrm{sgn}(\boldsymbol{s})\right) \le \boldsymbol{C}(\eta - k_1)\|\boldsymbol{s}\| < 0. \tag{18}$$

Thus, the stability of the HO-TSM surface can be ensured. According to (16) and (17), the system can converge to $\boldsymbol{s} = 0$ within t_2 in (13). By substituting $\boldsymbol{s} = 0$ into (16), $\boldsymbol{u}_n = -\boldsymbol{d}$ can be achieved. Thus, the system disturbance $\boldsymbol{d}$ can be offset by $\boldsymbol{u}_{\mathrm{n}}$ within t_2. This complete the proof.

Fig. 2 shows the block diagram of the conventional HO-TSM current controller. According to above analysis, there are two steps during the design of the controller.

1) The designed HO-TSM surface introduces the ideal convergence dynamic $\boldsymbol{s} = 0$. On this basis, the equivalent control term $\boldsymbol{u}_{eq}$ is designed to construct the convergence dynamic in undisturbed system.
2) The integral control term $\boldsymbol{u}_n$ is designed to compensate disturbance and drive the system back to $\boldsymbol{s} = 0$. Then, the system state can converge along the $\boldsymbol{s} = 0$ to the equilibrium point.

B. Advantages and Disadvantages of HO-TSM

Here, the HO-TSM current controller is evaluated by the three standards: strong robustness to the system disturbance; rapid convergence; and chattering suppression capability.

First, the anti-disturbance capability of the HO-TSM is analyzed. According to Theorem 1, if the restriction (13) is satisfied, the disturbance $\boldsymbol{d}$ can be effectively compensated by $\boldsymbol{u}_n$ within t_2. Thus, the HO-TSM controller can meet the requirement of strong robustness of the system disturbance.

Second, the convergence speed of the HO-TSM is evaluated. From (10), when the ideal convergence dynamic $\boldsymbol{s} = 0$ is achieved, the convergence time t_1 can be shortened by increasing the value of α. From (14), the convergence time of disturbance compensation t_2 can be shortened by increasing the value of integral control gain k_1. Thus, it can be concluded that the HO-TSM can possess rapid convergence capability at the cost of high value control gains α and k_1.

Third, the HO-TSM has certain chattering suppression capability compared. From (11), the continuous nonlinear function $|\boldsymbol{e}|^p\mathrm{sgn}(\boldsymbol{e})$ is applied, and the switching function is hidden in the derivate of control law $\boldsymbol{u}_n$. In continuous time, HO-TSM can achieve chattering free control theoretically [22]. However, the nonlinear function and $\boldsymbol{u}_n$ are unsmooth control term, so that the chattering is inevitable due to the discretization of digital control. Moreover, to ensure the rapid convergence, overlarge control gains α and k_1 is required, resulting in the aggravation of chattering problem.

In summary, the advantage of HO-TSM is that it can compensate system disturbance $\boldsymbol{d}$ within finite-time. Thus, the HO-TSM possesses the robustness to system disturbance.

The disadvantage of HO-TSM can be summarized as follows.

1) The only solution to achieve rapid convergence in HO-TSM is to select high value control gains α and k_1. Thus, the fast convergence capability needs improvement.
2) The high value gains of the unsmooth control term will result in the aggravation of chattering problem. Thus, the chattering suppression capability also need to be improved.

IV. Proposed Fast HO-TSM

In this section, the HO-TSM control structure is modified to improve its convergence speed and chattering suppression capability. The modifications of the HO-TSM surface, the control law, and the nonlinear gain of unsmooth integral term are provided, respectively.

A. Fast HO-TSM Surface Design

In order to increase the convergence speed of the designed convergence dynamic, a fast HO-TSM surface is designed

$$\boldsymbol{s}' = \frac{d\boldsymbol{e}}{dt} + \alpha|\boldsymbol{e}|^{(3+\mathrm{sgn}(|\boldsymbol{e}|-1))/4}\mathrm{sgn}(\boldsymbol{e}) + \beta\boldsymbol{e} \tag{19}$$

where $\alpha > 0$, $\beta > 0$ are the gains of the designed surface.

The designed convergence dynamic $\boldsymbol{s}' = 0$ is expressed as

$$d\boldsymbol{e}/dt = -\alpha|\boldsymbol{e}|^{(3+\mathrm{sgn}(|\boldsymbol{e}|-1))/4}\mathrm{sgn}(\boldsymbol{e}) - \beta\boldsymbol{e}. \tag{20}$$

Then, the segmented analysis of the convergence process is carried out as follows.

1) When system state is far away from the equilibrium ($\|\boldsymbol{e}\| \ge 1$), (20) can be rewritten as: $d\boldsymbol{e}/dt = -(\alpha+\beta)\boldsymbol{e}$. Here, the linear term can increase the slope of the system dynamic to achieve fast convergence. The system state will converge to $\|\boldsymbol{e}\| = 1$within finite-time: $\ln(\|\boldsymbol{e}(0)\|)/(\alpha+\beta)$.
2) When system state converges near to equilibrium ($\|\boldsymbol{e}\| < 1$), (20) can be rewritten as: $d\boldsymbol{e}/dt = -\alpha|\boldsymbol{e}|^{0.5}\mathrm{sgn}(\boldsymbol{e}) - \beta\boldsymbol{e}$. Here, the 0.5-power control term is necessary for the finite-time convergence. The system state will converge to $d\boldsymbol{e}/dt = \boldsymbol{e} = 0$ within finite-time: $2\ln(1+\beta/\alpha)/\beta$.

According to above analysis, the convergence time of new sliding mode surface t_3 is given as

$$t_3 = \frac{1}{(\alpha+\beta)}\ln\|\boldsymbol{e}(0)\| + \frac{2}{\beta}\ln\left(1+\frac{\beta}{\alpha}\right). \tag{21}$$

Thus, compared with conventional HO-TSM surface, the improvement of the novel sliding-mode surface is in following two aspects.

1) When the system is far away from the equilibrium, the linear term can effectively increase the convergence speed.
2) By increasing β, the convergence time (21) can be reduced, so that the high value of α is unnecessary. Since $\beta \boldsymbol{e}$ is a smooth control term, the chattering caused by high value gain β can be effectively avoided.

B. Control Law Modification

The control law of the HO-TSM is modified on the basis of the designed sliding-mode surface. First, the equivalent control term $\boldsymbol{u'}_{eq}$ is restructured according to (20). Second, the disturbance-compensate term is modified by a linear integral control term to shorten the regulation time of disturbance compensation. The control law of HO-TSM is redesigned as

$$\boldsymbol{u} = \boldsymbol{u'}_{eq} + \boldsymbol{u'}_{n}$$

$$\begin{cases} \boldsymbol{u'}_{eq} = -\boldsymbol{C}^{-1}\left(\boldsymbol{A}\boldsymbol{i}+\boldsymbol{B}+\alpha|\boldsymbol{e}|^{(3+\mathrm{sgn}(|\boldsymbol{e}|-1))/4}\mathrm{sgn}\left(\boldsymbol{e}\right)+\beta\boldsymbol{e}\right) \\ \dot{\boldsymbol{u}}'_{n} = -\left(k_1\mathrm{sgn}\left(\boldsymbol{s'}\right)+k_2\boldsymbol{s'}\right) \end{cases} \tag{22}$$

where $\boldsymbol{u'}_n(0) = 0$, $k_1 > \eta > \|\dot{\boldsymbol{d}}\|$, and $k_2 > 0$.

By substituting (22) into (4), the convergence dynamic of the HO-TSM can be expressed as

$$\begin{aligned} \frac{d\boldsymbol{e}}{dt} = & -\alpha|\boldsymbol{e}|^{(3+\mathrm{sgn}(|\boldsymbol{e}|-1))/4}\mathrm{sgn}\left(\boldsymbol{e}\right)-\beta\boldsymbol{e} \\ & +\boldsymbol{C}\left(\boldsymbol{d}-\int\left(k_1\mathrm{sgn}\left(\boldsymbol{s'}\right)+k_2\boldsymbol{s'}\right)dt\right) \end{aligned} \tag{23}$$

Theorem 2: The modified control law in (22) can compensate the system disturbance $\boldsymbol{d}$ (with initial condition $\boldsymbol{d}(0)$) in a finite-time t_4

$$t_4 \le \frac{1}{k_2}\ln\left(\frac{k_2}{k_1-\eta}\left\|\boldsymbol{d}\left(0\right)\right\|+1\right). \tag{24}$$

Proof: By substituting (4) into (19), it yields

$$\boldsymbol{s'} = \boldsymbol{A}\boldsymbol{i}+\boldsymbol{B}+\boldsymbol{C}\left(\boldsymbol{u}+\boldsymbol{d}\right)+\alpha|\boldsymbol{e}|^{(3+\mathrm{sgn}(|\boldsymbol{e}|-1))/4}\mathrm{sgn}\left(\boldsymbol{e}\right)+\beta\boldsymbol{e}. \tag{25}$$

Further substituting (22) into (25), we can obtain

$$\boldsymbol{s'} = \boldsymbol{C}\left(\boldsymbol{d}+\boldsymbol{u'}_n\right) \tag{26}$$

$$\dot{\boldsymbol{s}}' = \boldsymbol{C}\left(\dot{\boldsymbol{d}}-k_1\mathrm{sgn}\left(\boldsymbol{s'}\right)-k_2\boldsymbol{s'}\right) \le \boldsymbol{C}\left(\eta-k_1\mathrm{sgn}\left(\boldsymbol{s'}\right)-k_2\boldsymbol{s'}\right). \tag{27}$$

To analyze the stability of the improved HO-TSM, a Lyapunov function is considered: $V' = 0.5\,\boldsymbol{s'}^T\boldsymbol{s'}$. The derivative of V' with respect to time is: $\dot{V}' = \boldsymbol{s'}^T\dot{\boldsymbol{s}}'$. By substituting (27) into $\dot{V}'$, it can be obtained that

$$\begin{aligned} \boldsymbol{s'}^T\dot{\boldsymbol{s}}' &= \boldsymbol{C}\left(\boldsymbol{s'}^T\dot{\boldsymbol{d}}-k_1\boldsymbol{s'}^T\mathrm{sgn}\left(\boldsymbol{s'}\right)-k_2\boldsymbol{s'}^T\boldsymbol{s'}\right) \\ &\le \boldsymbol{C}\left(\eta-k_1\right)\|\boldsymbol{s'}\|-\boldsymbol{C}k_2\boldsymbol{s'}^T\boldsymbol{s'} < 0. \end{aligned} \tag{28}$$

Thus, $\boldsymbol{s'} = 0$ can be guaranteed within finite-time. Assuming $\boldsymbol{s'}(0) = \boldsymbol{C}\boldsymbol{d}(0) > 0$, by solving the (27), we can get

$$\boldsymbol{s'}\left(t\right) = \left(\boldsymbol{s'}\left(0\right)+\boldsymbol{C}\frac{k_1-\eta}{k_2}\right)\mathrm{e}^{-k_2t}-\boldsymbol{C}\frac{k_1-\eta}{k_2}. \tag{29}$$

By solving the above equation, the integral control term the $\boldsymbol{u'}_n$ can compensate the system disturbance $\boldsymbol{d}$ within t_4, so that the system will converge to $\boldsymbol{s'} = 0$. This complete the proof.

Thus, compared with conventional HO-TSM, the improvement of the control law is as following.

1) Compared (14) with (24), with proper selection of the gains k_1 and k_2, the modified control law can increase the speed of disturbance compensation.
2) The add integrator $k_2\int\boldsymbol{s'}dt$ is a smooth control term, so that the chattering caused by high value gain k_2 can be avoided.

To clarify the effectiveness of the above modifications, the convergence dynamic of improved HO-TSM in (23) is compared with that of the conventional HO-TSM in (12) by simulation. The system initial state and parameter is: $\boldsymbol{e}(0) = -3$ and $\boldsymbol{C} = 92.96$. The control gains of the conventional HO-TSM is selected as: $\alpha = 1.5$; $p = 0.5$; and $k_1 = 5$. The control gains of the proposed HO-TSM is selected as: $\alpha = 1.5$; $\beta = 0.5$; $k_1 = 5$; and $k_2 = 3$. Two different system disturbances are adopted: (case. 1), $\boldsymbol{d} = 3+0.5t+0.05\sin(10t)$; (case. 2), $\boldsymbol{d} = -3-0.5t-0.05\sin(10t)$. Figs. 3 and 4 show the convergence dynamic of the conventional HO-TSM and the studied fast HO-TSM, respectively. From waveform of the convergence trajectory, both of the methods have two-stage convergence behavior.

1) Approaching stage, where the disturbance can be compensated so that the system can converge to $\boldsymbol{s} = 0$, or $\boldsymbol{s'} = 0$.
2) Sliding stage, where the system can converge along the designed convergence dynamic. From system responses of case. 1 and case. 2, both the approaching stage and sliding stage can be accelerated by the proposed method. Thus, the modification of the sliding-mode surface and the control law can maintain the disturbance compensation capability, and improve the system convergence speed effectively.

C. Chattering Suppression of Modified Control Law

From (22), the $\boldsymbol{u'}_n$ can be rewritten in integrator form:

$$\boldsymbol{u'}_n = -k_1\int\mathrm{sgn}\left(\boldsymbol{s'}\right)dt-k_2\int\boldsymbol{s'}dt. \tag{30}$$

According to the analysis of Figs. 3 and 4, the added linear integrator $k_2\int\boldsymbol{s'}dt$ can effectively accelerate the disturbance compensation. However, the nonlinear integrator $k_1\int\mathrm{sgn}(\boldsymbol{s'})dt$ is still necessary to stabilize the controller by satisfying $k_1 > \eta > \|\dot{\boldsymbol{d}}\|$. Then, the chattering caused by $k_1\int\mathrm{sgn}(\boldsymbol{s'})dt$ still exists during steady-state.

From the analysis of (6) and (7), during transient state, the stability boundary $\eta > 0$. Here, the high value gain k_1 is required for finite-time compensation of disturbance $\boldsymbol{d}$. During steady state, the stability boundary $\eta = 0$, which means that the high value gain k_1 is no longer necessary.

Based on this idea, the constant gain k_1 is replaced by a variable nonlinear gain. The final form of proposed HO-TSM

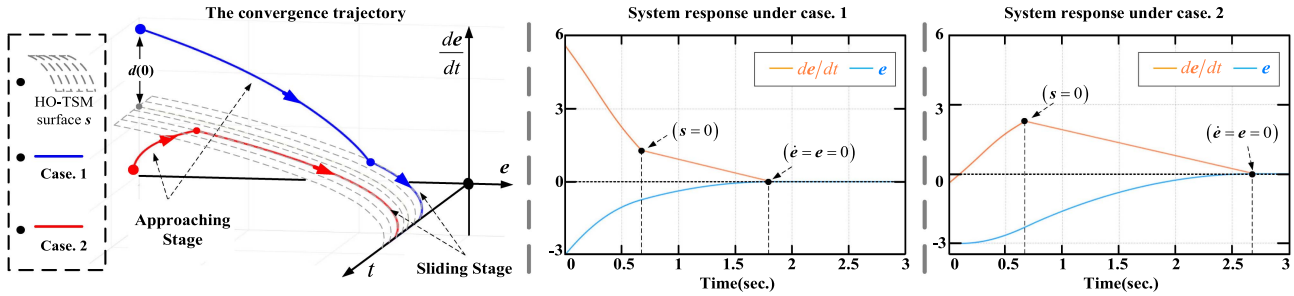

Fig. 3. Convergence dynamic of the conventional HO-TSM.

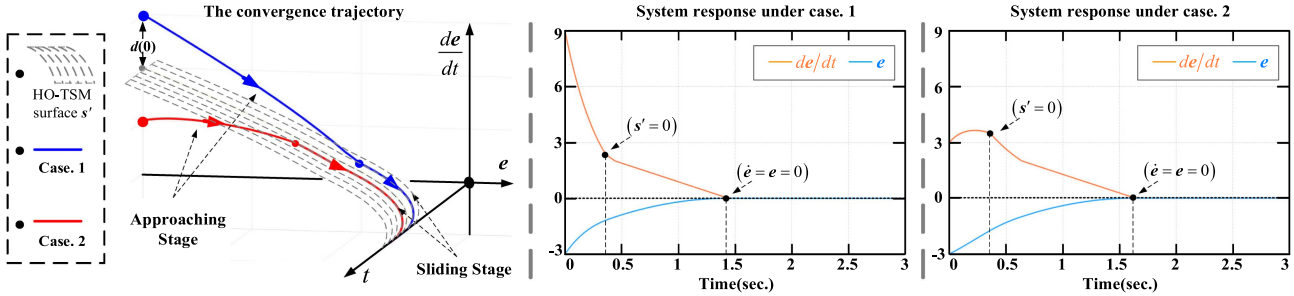

Fig. 4. Convergence dynamic of the proposed fast HO-TSM.

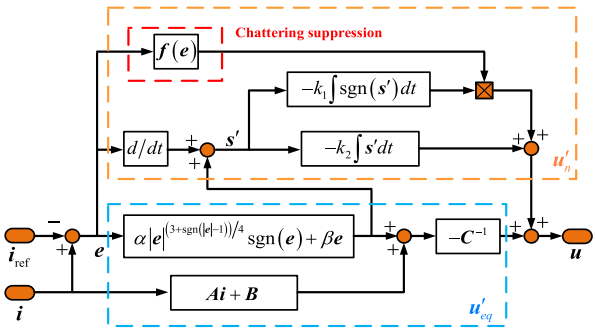

Fig. 5. Block diagram of designed HO-TSM current controller.

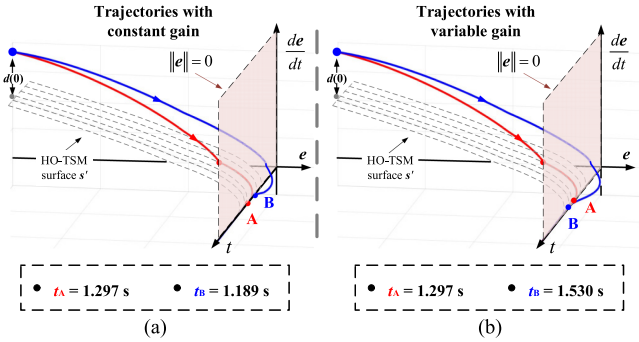

Fig. 6. Convergence dynamic of proposed HO-TSM. (a) With constant gain. (b) With variable gain.

is redesigned as

$$\begin{cases} \boldsymbol{u'}_{eq} = -\boldsymbol{C}^{-1}\left(\boldsymbol{Ai}+\boldsymbol{B}+\alpha|\boldsymbol{e}|^{(3+\mathrm{sgn}(|\boldsymbol{e}|-1))/4}\mathrm{sgn}\,(\boldsymbol{e})+\beta\boldsymbol{e}\right) \\ \boldsymbol{u'}_{n} = -\left(k_1 f\,(\boldsymbol{e})\int \mathrm{sgn}\,(\boldsymbol{s'})\,dt + k_2\int \boldsymbol{s'}dt\right) \end{cases} \tag{31}$$

$$f\,(\boldsymbol{e}) = \min\left\{\|\boldsymbol{e}\|/\xi, 1\right\} \tag{32}$$

where ξ is the threshold of saturation function. In this article, ξ is selected as 0.5 A. According to (31) and (32), Fig. 5 shows the diagram of designed HO-TSM current controller.

First, the impact of variable gain on the stability is analyzed. In Fig. 4, the disturbance will first be compensated when $\boldsymbol{s'} = 0$ is achieved, and then the system will converge to equilibrium point $\dot{\boldsymbol{e}} = \boldsymbol{e} = 0$. Thus, when the system converges to equilibrium point (judged by $\|\boldsymbol{e}\| < \xi$), the disturbance has already been compensated, so the chattering caused by integrator $k_1\int \mathrm{sgn}(\boldsymbol{s'})dt$ can be eliminated as $\|\boldsymbol{e}\|$ converges to zero. Thus, during the steady state, by substituting $\eta = 0$ and $\|\boldsymbol{e}\| = 0$ into (28), it yields

$$\boldsymbol{s'}^{T}\dot{\boldsymbol{s}}' \le (\eta - k_1\boldsymbol{f}\,(\boldsymbol{e}))\,\|\boldsymbol{s'}\| - k_2\boldsymbol{s'}^{T}\boldsymbol{s'} < -k_2\boldsymbol{s'}^{T}\boldsymbol{s'} < 0. \tag{33}$$

This means that after the disturbance $\boldsymbol{d}$ is compensated, the other integrator $k_2\int \boldsymbol{s'}dt$ in $\boldsymbol{u}_n{}'$ can force the system stay on the sliding-mode surface, ensuring the stability at steady state. Therefore, by introducing nonlinear gain $k_1 f(\boldsymbol{e})$, the chattering suppression capability can be further improved.

On the other hand, the influence of variable gain on the convergence time is analyzed with the simulation result in Fig. 6. Here, the system initial state and disturbance are selected as: $\boldsymbol{e}(0) = -3$, and $\boldsymbol{d} = 5 + 3e^{-10t}$. The gains in sliding-mode surface are designed as: $\alpha = 1.5$, $\beta = 0.5$. Then, in Fig. 6(a), the constant

gains are adopted: for the red curve $k_1 = 10$, and $k_2 = 3$ and for the blue curve $k_1 = 2$, and $k_2 = 3$. In Fig. 6(b), the variable gains are adopted: for the red curve $k_1 = 10f(\boldsymbol{e})$, and $k_2 = 3$ and for the blue curve $k_1 = 2f(\boldsymbol{e})$, and $k_2 = 3$.

The convergence time to $\boldsymbol{s}' = 0$ with constant gain can be expressed as (29). Here, by replacing the constant gain k_1 with $k_1 \min\{\|\boldsymbol{e}\|/\xi, 1\}$, the gain value will remain constant if $\|\boldsymbol{e}\| > \xi$, and it will be decreased when $\|\boldsymbol{e}\| < \xi$. From the blue curves of Fig. 6, the gains value is low and the convergence trajectory will pass through the $\|\boldsymbol{e}\| = 0$. Thus, the gain value will be decreased and the convergence time will be enlarged. Then, the convergence time t_B of variable gain is longer than it with constant gain. From the red curves of Fig. 6, by increasing the value of k_1, it can be seen that the system can converge to the sliding-mode surface $s' = 0$ before the current error converges within $\|\boldsymbol{e}\| < \xi$. Here, the convergence time t_A of Fig. 6(a) and (b) are the same. Thus, if the system can achieve to $s' = 0$ before the current error converges within $\|\boldsymbol{e}\| < \xi$, the variable gain will not affect the overall convergence time.

V. Implementation of HO-TSM Current Controller

According to above analysis, the studied fast HO-TSM can maintain the strong robustness of disturbance, and effectively improve the capability of rapid convergence and chattering suppression. Then, the important implementation details are given in this section.

A. Implementation of Modified Control Law

It is evident that the disturbance-compensate term $\boldsymbol{u}_n{}'$ plays an essential role in the proposed method. From (31), the value of $\boldsymbol{s}'$ is required for the calculation of $\boldsymbol{u}_n{}'$.

However, the sliding mode surface $\boldsymbol{s}'$ contain the derivative of current error $\dot{\boldsymbol{e}}$, which is neither measurable nor calculable. This means that the exact value of $\boldsymbol{s}'$ is not available for $\boldsymbol{u}_n{}'$ calculation. To address this problem, the calculation method of $\boldsymbol{u}_n{}'$ is provided.

First, according to (19), the integrator $\int \boldsymbol{s}'dt$ can be written as

$$\int \boldsymbol{s}'dt = \boldsymbol{h}(t) = \boldsymbol{e} + \alpha \int |\boldsymbol{e}|^{(3+\mathrm{sgn}(|\boldsymbol{e}|-1))/4} \mathrm{sgn}(\boldsymbol{e})\, dt + \beta \int \boldsymbol{e}dt. \tag{34}$$

Second, $\mathrm{sgn}(\boldsymbol{s}')$ only needs the sign of $\boldsymbol{s}'$. Thus, based on discrete control property, $\mathrm{sgn}(\boldsymbol{s}')$ can be rewritten as [23], [25]

$$\mathrm{sgn}(\boldsymbol{s}') = \mathrm{sgn}\left(\lim_{\tau \to 0} \frac{\boldsymbol{h}(t) - \boldsymbol{h}(t-\tau)}{\tau}\right) \tag{35}$$

where τ is the is the sampling period of the control system. Since $\tau > 0$, (35) can be rewritten as

$$\mathrm{sgn}(\boldsymbol{s}') = \mathrm{sgn}(\boldsymbol{h}(t) - \boldsymbol{h}(t-\tau)). \tag{36}$$

By substituting (34) and (36) into (31), the disturbance-compensate term $\boldsymbol{u}_n{}'$ can be calculated by

$$\boldsymbol{u'}_n = k_1 f(\boldsymbol{e}) \int \mathrm{sgn}(\boldsymbol{h}(t) - \boldsymbol{h}(t-\tau))\, dt + k_2 \boldsymbol{h}(t). \tag{37}$$

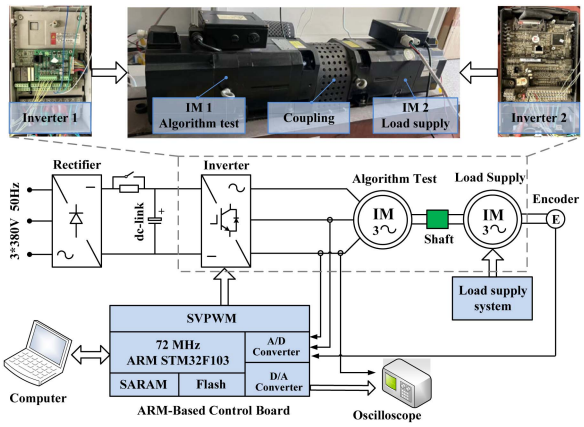

Fig. 7. Block diagram of the experimental setup.

Thus, the $\boldsymbol{u}_n{}'$ can be calculated without exact value of $\boldsymbol{s}'$.

B. Control Gains Selection

There are four control gains need to be tuned in the proposed HO-TSM current controller. Control gains α and β are in the designed sliding-mode surface (19). The other two control gains k_1 and k_2 are in the modified control law (31). Thus, the four control gains are divided into two group for gains tuning.

The control gains α and β determine the convergence time of stator current under undisturbed condition t_3. From (21), the larger value of α and β can obtain shorter convergence time. Considering an expected convergence time of stator current t_0, a crude selecting range of α and β can be obtained by satisfying $t_3 < t_0$ [21]. According to the previous analysis in this article, high value of α will increase the chattering problem because of the unsmooth function. Then, the control gain β should occupy the bigger part of the selection range. Thus, the control gains α and β can be selected by considering both the convergence time and the chattering suppression.

The control gains $k1$ and $k2$ determine the disturbance compensation time $t4$. In the ideal undisturbed system, the system convergence time is determined by the convergence time of the sliding-mode surface t_3. However, in the actual disturbed system, according to convergence dynamic in Fig. 4, the disturbance will first be compensated by the integral control law within t_4, and then the current error will converge along the sliding-mode surface. If the disturbance compensation time t_4 is longer than the ideal convergence time t_3, it is evident that the overall convergence time will also be longer than the ideal convergence time, resulting in the convergence delay [2]. Thus, in order to ensure the fast convergence of the proposed HO-TSM, the convergence time of the new sliding mode surface need to be set as the upper limit of convergence time to direct the selection of the control gains. According to (21) and (24), for convenience of calculation, the $t_4 < t_3$ can be rewritten as

$$t_4 < \frac{\|\boldsymbol{d}(0)\|}{k_1 - \eta} < \frac{1}{(\alpha + \beta)} \ln \|\boldsymbol{e}(0)\| < t_3. \tag{38}$$

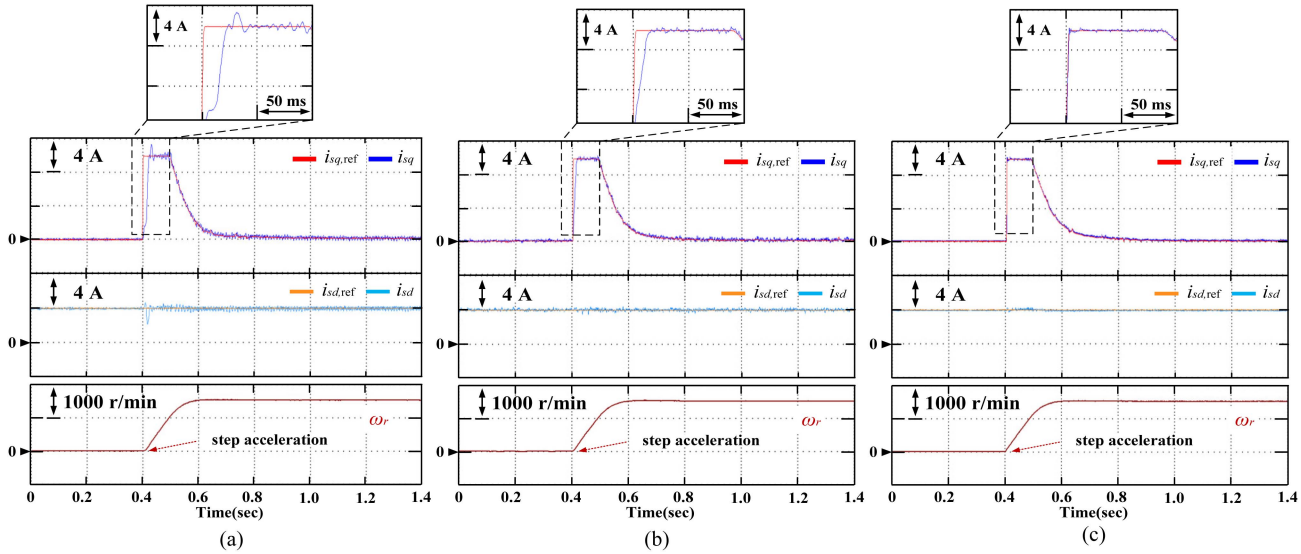

Fig. 8. System response during IM step acceleration (0 r/min to 1500 r/min) without load. From top to bottom: q-axis stator current i_{sq} & $i_{sq,\mathrm{ref}}$, d-axis stator current i_{sd} & $i_{sd,\mathrm{ref}}$, and rotor speed ω_r. (a) Conventional STA, (b) conventional HO-TSM, and (c) proposed HO-TSM.

TABLE I
INDUCTION MOTOR PARAMETERS

Parameter	Value	Parameter	Value
Rated power	3.7 kW	Stator resistance	1.142 Ω
Rated current	8.9 A	Rotor resistance	0.825 Ω
Rated voltage	380 V	Stator/rotor inductance	0.1244 H
Rated speed	1500 rpm	Mutual inductance	0.1189 H
Rated frequency	50 Hz	Number of pole pairs	2

Thus, the selecting range of k_1 is obtained. From (24), by increasing k_2, the disturbance can be offset faster. Then the selecting principle of k_1 and k_2 in this article is given as

$$k_2 = k_1 > \frac{\|\boldsymbol{d}(0)\|}{\ln\|\boldsymbol{e}(0)\|}(\alpha+\beta)+\eta. \tag{39}$$

Thus, the four control gains of proposed HO-TSM current controller can be selected by the above description of gains tuning process.

VI. EXPERIMENTAL RESULT

The proposed fast HO-TSM current controller has been realized on a 3.7 kW IM test bench shown in Fig. 7. The experimental setup is composed of:

1) Two identical IMs, with parameters given in Table I, are connected by flexible coupling. Each motor is driven by an inverter, and these two inverters are connected to a common dc-bus. The IM 1 adopts the FOC in Fig. 1 to test the algorithm. The IM 2 works at torque mode to provide load torque.
2) The proposed algorithm (see Fig. 1) is implemented on an ARM-based control board. The adopted STM32F103 ARM is a 32-bit fixed-point microcontroller with 72 MHz of maximum operating frequency. Two phases are used for current measurement with A/D converters. The A/D converters are applied to sampling experimental waveforms. The symmetrical SVPWM strategy is applied. By considering the switching loss of the controller and the performance of the control algorithm, the switching frequency is selected as 6 kHz. The sampling period of the control system τ is 166.7 μs.

In this article, three different IM current controller are tested to form the contrast experiments.

1) The STA controller in [21].
2) The conventional HO-TSM current controller in (11).
3) The proposed HO-TSM current controller in (31).

The control gains of super-twisting controller are selected by the analysis in [21]. The gains of the conventional HO-TSM controller and proposed HO-TSM controller are selected by the analysis of *Control Gains Selection* in this article: $\alpha = 120$, and $k_1 = 4800$ are selected for the conventional HO-TSM; $\alpha = 75$, $\beta = 125$, $k_1 = k_2 = 3600$ are selected for the proposed HO-TSM.

A. Dynamic Performance Contrast Experiments

The rapid convergence capability is first tested. Fig. 8 shows the system response of IM during start up with three different current controllers. The IM works at 0 r/min and step accelerate to 1500 r/min at 0.4 s. The current reference value $i_{sq,\mathrm{ref}}$ change to 10 A (current limit value) immediately at 0.4 s.

From Fig. 8(a), with STA current controller, the regulation time of i_{sq} is 27.4 ms, and there also appears current overshoot of 1.1 A. The current fluctuation of i_{sd} can be found in the figure of d-axis current. In Fig. 8(b), the current overshoot can be effectively suppressed, and the regulation time is reduced to 16 ms. Thus, the conventional HO-TSM can improve the current transient performance compared with conventional STA. In the enlarged figure in Fig. 8(c), the current regulation time can be further reduced to 1.3 ms by the proposed fast HO-TSM.

Fig. 9 shows the system response during acceleration with load and load sudden change. The IM first works at 300 r/min

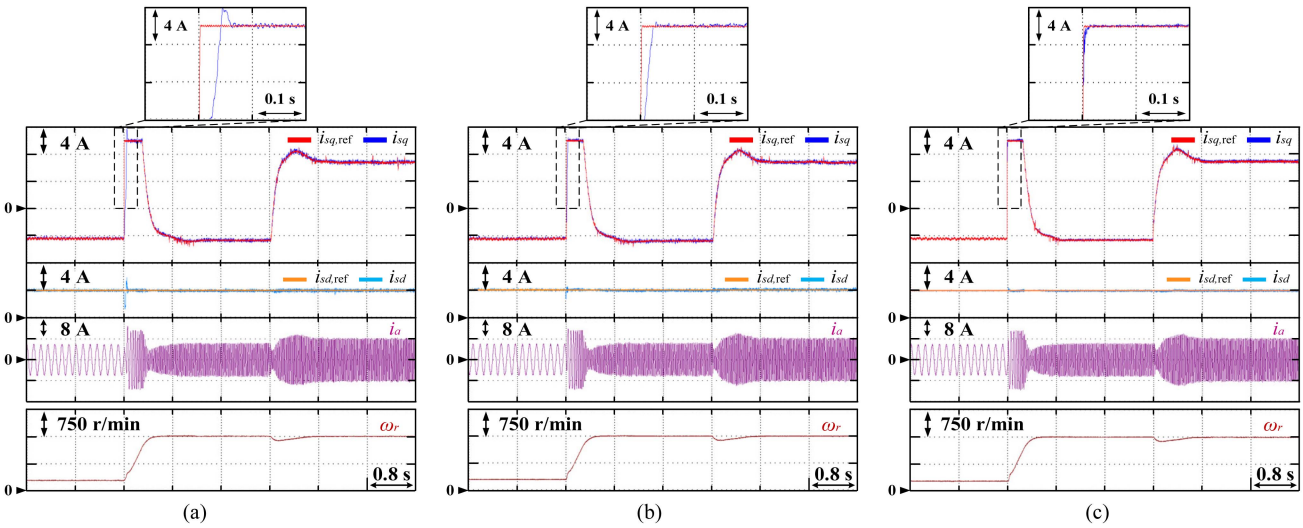

Fig. 9. System response under start-up and sudden load variation. From top to bottom: q-axis stator current i_{sq} & $i_{sq,\mathrm{ref}}$, d-axis stator current i_{sd} & $i_{sd,\mathrm{ref}}$, a-phase current i_a, and rotor speed ω_r. (a) Conventional STA. (b) Conventional HO-TSM. (c) Proposed HO-TSM.

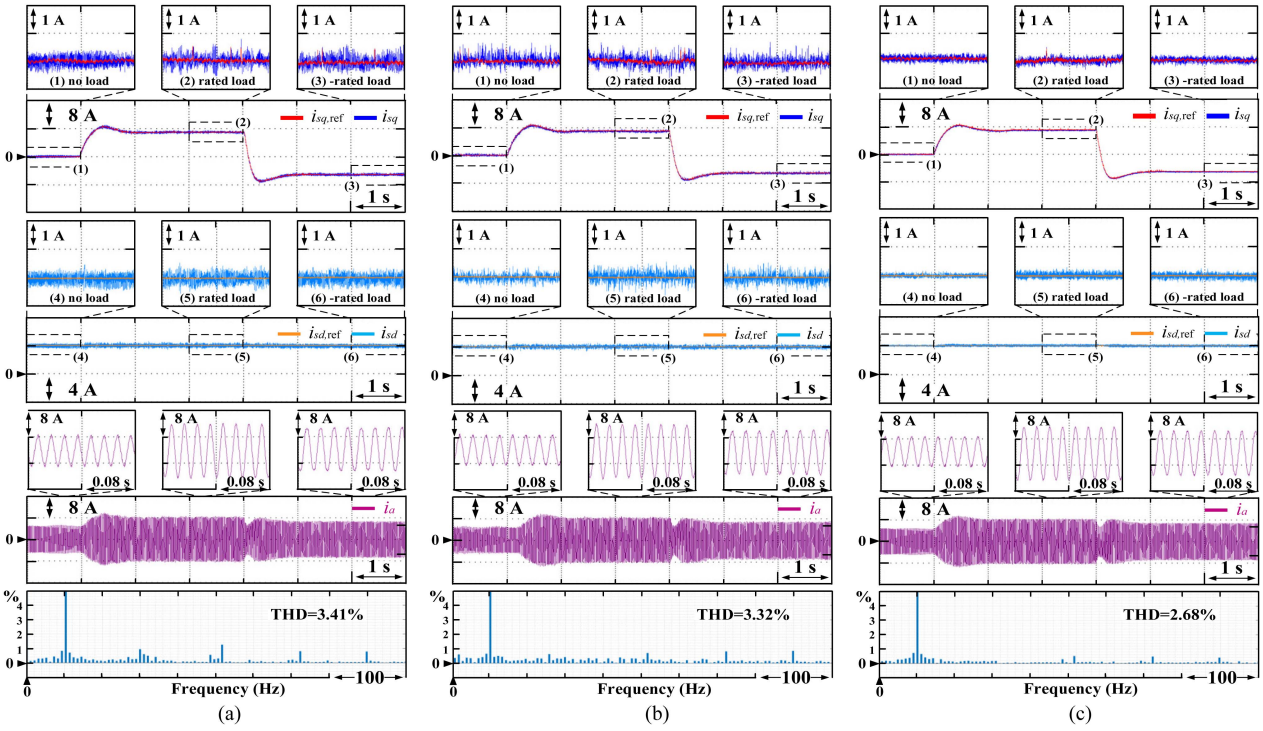

Fig. 10. System response during load torque change [0 to 21 N·m (rated load), and to -21 N·m]. From top to bottom: q-axis stator current i_{sq} & $i_{sq,\mathrm{ref}}$, and its local enlarged figure; d-axis stator current i_{sd} & $i_{sd,\mathrm{ref}}$, and its local enlarged figure, a-phase current i_a, and the its Fourier analysis. (a) Conventional STA. (b) Conventional HO-TSM. (c) Proposed HO-TSM.

with load of -80% rated load, and then at 1.6 s, the IM step accelerates to 1500 r/min with load. Then, at 4 s, the load changes from -80% to $+100\%$ rated load.

According to the waveform of i_{sq}, the convergence performance during load torque sudden change can be ensured with all three methods, but the performance at sudden speed change are different. In Fig. 9(a), the conventional STA has the longest regulation time of i_{sq}, and there also exists current overshoot. In Fig. 9(b), the regulation time can be reduced to 20 ms, and the current overshoot can be suppressed. In Fig. 9(c), the current regulation time can be further reduced to 5.4 ms. Therefore, this set of experiments can verify the improvement of rapid convergence capability by the proposed method.

B. *Chattering Suppression Contrast Experiments*

Fig. 10 shows the system response during load torque change with three different methods. The IM works at 1500 r/min, then the external load change to 21 N·m (rated load) at 1 s, and change

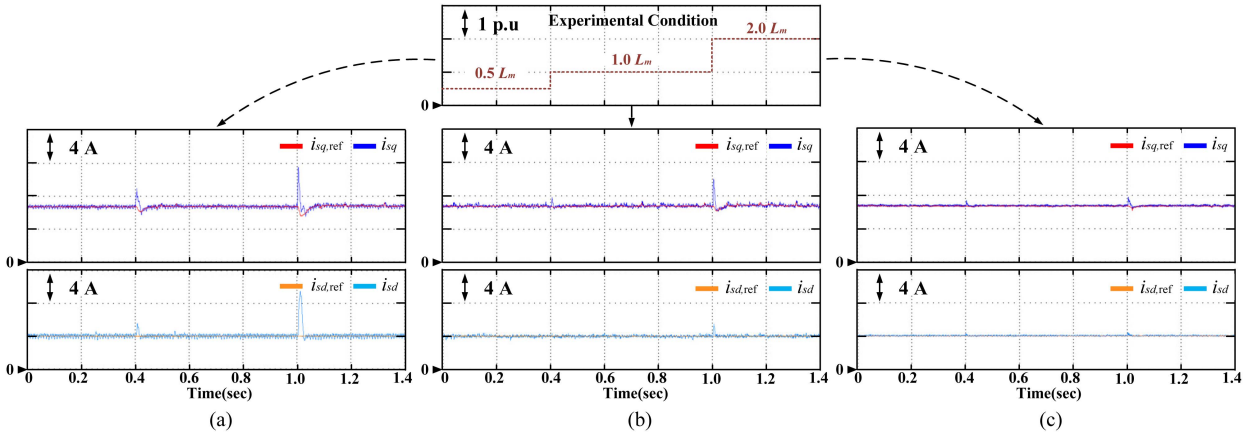

Fig. 11. System response under L_m variation (0.5 to 1.0, and to 2.0 of its rated value). From top to bottom: q-axis stator current i_{sq} & $i_{sq,\mathrm{ref}}$, d-axis stator current i_{sd} & $i_{sd,\mathrm{ref}}$. (a) Conventional STA. (b) Conventional HO-TSM. (c) Proposed HO-TSM.

to -21 N·m at 4 s. The enlarge figure can shows the size of chattering under no load, rated load, and reverse rated load.

It shows that all three methods can achieve accurate current tracking performance under load sudden change. However, in the enlarge figure of Fig. 10(a) and (b), although the STA and HO-TSM have both been claimed to possess the chattering suppression capability in [22] and [23], there are still room for improvement. According to the phase current waveform and its Fourier analysis results, the chattering will result in the current harmonics. By contrast in the enlarge figure of Fig. 10(c), the chattering amplitude can be reduced by the proposed method, mainly caused by the variable nonlinear gain in modified control law. Then, in the Fourier analysis of Fig. 10(c), the current harmonics can be effectively suppressed, so that the THD can be reduced. Therefore, the proposed HO-TSM can meet the requirement of chattering suppression capability.

C. Antidisturbance Capability Contrast Experiments

This part evaluates the robustness to system disturbance by comparing current control performance of different methods under IM parameter variations.

In Fig. 11, the IM works under rated load at 1500 r/min. The mutual inductance *Lm* changes from 0.5 to 1.0 and to 2.0 of its rated value. Here, the experimental condition of parameter abrupt change is simulated by changing its value in the program code [26]. From Fig. 11(a), the L_m sudden variation results in current error in both *dq*-axis. The maximum current error of STA current controller in *dq*-axis are 5.3 and 4.7 A, respectively. In Fig. 11(b), the maximum current errors are reduced to 1.3 and 3.2 A, which means the anti-disturbance capability can be improved by the conventional HO-TSM. This consist with the disturbance compensation capability of HO-TSM. In Fig. 11(c), the maximum current errors are further reduced to 0.5 and 1.1 A. Thus, the proposed fast HO-TSM can effectively enhance the anti-disturbance capability.

In Fig. 12, the IM works at 1500 r/min under rated load. The resistances R_s and R_r change from 1.0 to 2.0 of their rated value at 0.4 s. In Fig. 12(a), the resistances variation causes the severe current fluctuation of conventional STA. In

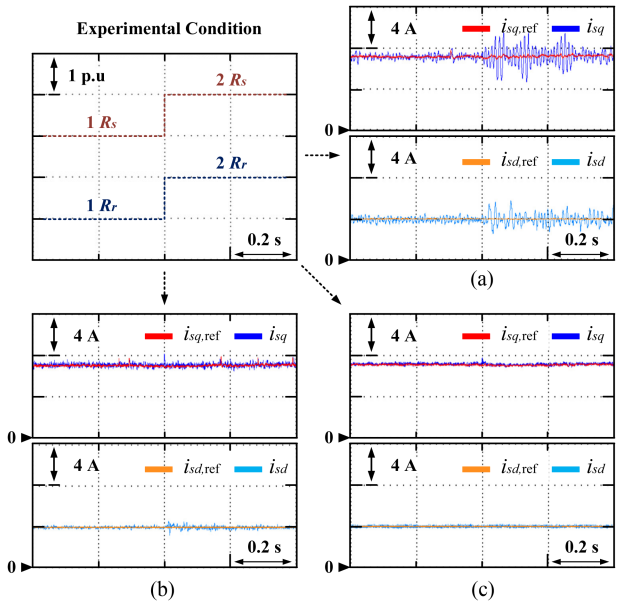

Fig. 12. System response under R_s, R_r variations (1.0 to 2.0 of their rated value). From top to bottom: q-axis current i_{sq} & $i_{sq,\mathrm{ref}}$, and d-axis current i_{sd} & $i_{sd,\mathrm{ref}}$.

Fig. 12(b), the current fluctuation can be effectively reduced by the conventional HO-TSM, but the current fluctuation in i_{sd} still cannot be eliminated. In Fig. 12(c), the proposed HO-TSM can further suppress the current fluctuation cause by the parameters variations. Therefore, the proposed method can meet the requirement of strong robustness to the system disturbance.

D. Contrast Experiments With PI Current Controller

Fig. 13 shows the comparative experimental results between the PI controller and the proposed HO-TSM under parameters mismatch. The IM step accelerates to 300 and 900 r/min at 1 and 3 s, respectively, and then reverse the -900 r/min at 5 s. For the PI current controller, the feedback decoupling term is applied [5], and its control bandwidth is selected as 300 Hz. In Fig. 13(a), with accurate IM parameters, the PI controller can

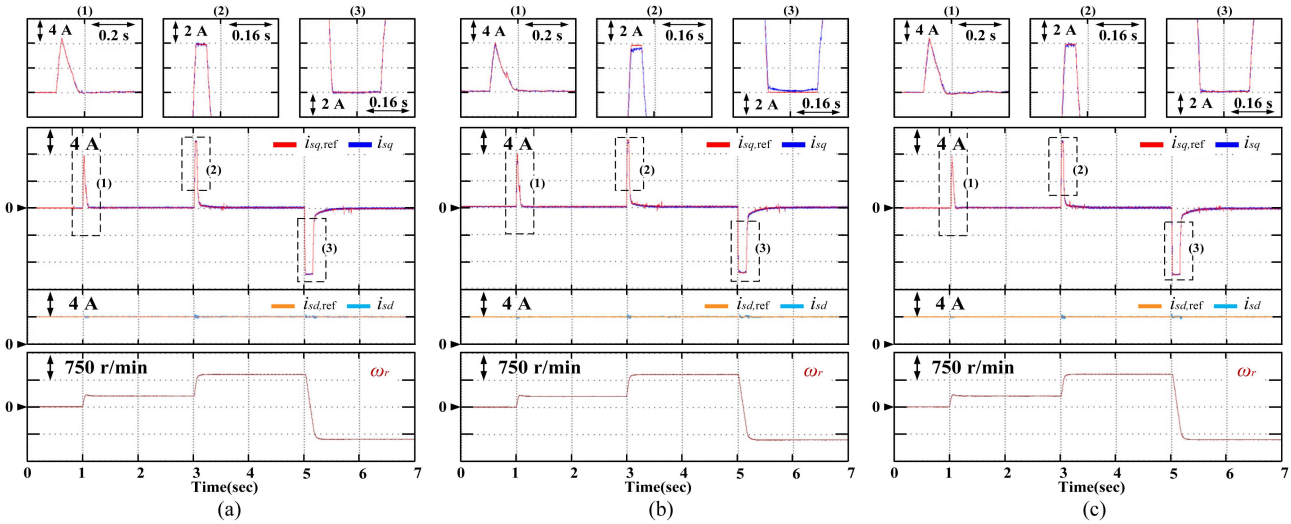

Fig. 13. System response during IM speed variation (0 to 300 r/min to 900 to −900 r/min) with IM parameters mismatch. From top to bottom: q-axis stator current i_{sq} & $i_{sq,\mathrm{ref}}$, d-axis stator current i_{sd} & $i_{sd,\mathrm{ref}}$, and rotor speed ω_r. (a) PI controller, with accurate parameter. (b) PI controller, with 0.5 R_s, 0.5 L_m. (c) Proposed HO-TSM, with 0.5 R_s, 0.5 L_m.

TABLE II
EXECUTION TIME OF DIFFERENT CURRENT CONTROLLERS

Methods	Algorithm	Number	Computing time
Conventional STA current controller	+, −	12	7.72 μs
	*, /	14	
	sqrt	2	
Conventional HO-TSM current controller	+, −	16	8.43 μs
	*, /	16	
	sqrt	2	
Proposed fast HO-TSM current controller	+, −	20	9.61 μs
	*, /	26	
	sqrt	2	

possess satisfactory current control performance. However, in Fig. 13(b), under parameters mismatch (0.5 R_s and 0.5 L_m), the current tracking performance of PI controller is degraded. In Fig. 13(c), the proposed HO-TSM can still ensure the satisfactory current control performance under parameters mismatch. Here, for current regulation, the PI gains are determined by the frequency domain index: bandwidth, and its effectiveness is on the basis of accurate IM parameters. For the proposed HO-TSM, its gains are determined by the time domain index: convergence time, and its value is determined by initial current error and the boundary of system disturbance. With proper gain selection based on the disturbance boundary, the HO-TSM can effectively compensate the external disturbance, and the system parameter variation will not have significant impact to control performance. Thus, the robustness of IM parameters can be improved by the studied method.

E. Comparison of Required Execution Time

Table II gives the comparison of the execution time of the different sliding-mode-based current controllers. Here, the conventional STA current controller has the minimum computational burden. In the existing HO-TSM, the extra calculation of sign(s) is required so that the its execution time is slightly higher than the STA. In the sliding-mode surface of proposed fast HO-TSM, the variable power term can be implemented with piecewise functions, so that the no extra power function calculation is required. It can be seen that the computing time of proposed HO-TSM is longer than that of the two existing current controllers. Nevertheless, the execution time 9.61 μs is much shorter than the control period 1/6000 s. Thus, the studied method is practicable for the adopted microcontroller.

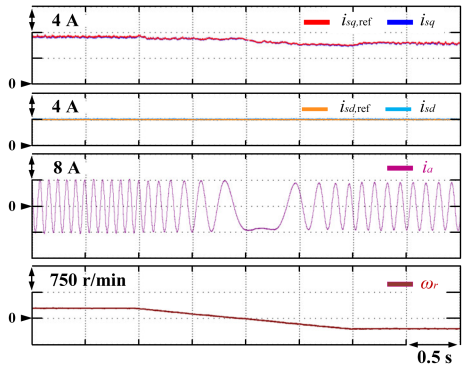

Fig. 14. System response under speed reversal with proposed fast HO-TSM (10 to −10 Hz, with rated load). From top to bottom: q-axis stator current i_{sq} & $i_{sq,\mathrm{ref}}$, d-axis stator current i_{sd} & $i_{sd,\mathrm{ref}}$, a-phase current i_a, and rotor speed ω_r.

F. Verification Experiments Under Speed Reversal

Fig. 14 shows the system response of proposed method under speed reversal. First, the IM works at 10 Hz with rated load. Then, at 1s, the reference speed begins to ramp down, and reverse to −10 Hz at 3 s. It can be seen that the stator current can track its reference correctly under slow speed variation. Here, from

the waveform of rotor speed, the proposed method can ensure the smooth speed reversal.

VII. Conclusion

The research focus of this article is to design a current controller with three characteristics: strong robustness to disturbance; fast convergence; and chattering suppression. By analyzing the system convergence process, it reveals that the conventional HO-TSM has the capability to compensate disturbance during the approaching stage, which meets the request of strong robustness. However, due to the unsmooth control terms, the conventional HO-TSM cannot achieve fast convergence without aggravating the chattering of current control. In contrast, the proposed fast HO-TSM solves this problem because of the modifications in following three aspects.

1) The designed fast sliding mode surface effectively accelerates the sliding stage with smooth control term, and maintain the finite-time convergence with fractional power control term.
2) The control law is augmented with a smooth integral term, which can shorten the disturbance compensation time.
3) The nonlinear gain, introduced into the control law, can get rid of the high value control gains when the system is in steady state, leading to more effective chattering suppression. Thus, the proposed HO-TSM can satisfy the requirements of strong robustness, fast convergence, and chattering suppression. The effectiveness of studied method is confirmed by the contrast experiments on a 3.7 kW IM platform.

References

[1] G. Sala, M. Mengoni, G. Rizzoli, L. Zarri, and A. Tani, "Decoupled d–q axes current-sharing control of multi-three-phase induction machines," *IEEE Trans. Ind. Electron.*, vol. 67, no. 9, pp. 7124–7134, Sep. 2020.

[2] B. Wang, T. Wang, Y. Yu, C. Luo, and D. Xu, "Convergence trajectory optimization of Super-twisting sliding-mode current control for induction motor drives," *IEEE Trans. Ind. Electron.*, vol. 69, no. 12, pp. 12292–12304, Dec. 2022.

[3] L. Wang, J. Mishra, Y. Zhu, and X. Yu, "An improved sliding-mode current control of induction machine in presence of voltage constraints," *IEEE Trans. Ind. Inform.*, vol. 16, no. 2, pp. 1182–1191, Feb. 2020.

[4] M. Tian, B. Wang, Y. Yu, Q. Dong, and D. Xu, "Discrete-Time repetitive control-based ADRC for current loop disturbances suppression of PMSM drives," *IEEE Trans. Ind. Inform.*, vol. 18, no. 5, pp. 3138–3149, May 2022.

[5] S. K. Sul, *Control of Electric Machine Drive Systems*. New York, NY, USA: Wiley, 2011.

[6] X. Zhang, B. Hou, and Y. Mei, "Deadbeat predictive current control of permanent-magnet synchronous motors with stator current and disturbance observer," *IEEE Trans. Power Electron.*, vol. 32, no. 5, pp. 3818–3834, May 2017.

[7] Y. Kali et al., "Time delay estimation based discrete-time super-twisting current control for a six-phase induction motor," *IEEE Trans. Power Electron.*, vol. 35, no. 11, pp. 12570–12580, Nov. 2020.

[8] Z. Yin, X. Han, C. Du, J. Liu, and Y. Zhong, "Research on model predictive current control for induction machine based on immune-optimized disturbance observer," *IEEE J. Emerg. Sel. Topics Power Electron.*, vol. 6, no. 4, pp. 1699–1710, Dec. 2018.

[9] Y. Ma, D. Li, Y. Li, and L. Yang, "A novel discrete compound integral terminal sliding mode control with disturbance compensation for PMSM speed system," *IEEE/ASME Trans. Mechatronics*, vol. 27, no. 1, pp. 549–560, Feb. 2022.

[10] T. Wang, B. Wang, Y. Yu, and D. Xu, "High-Order sliding-mode observer with adaptive gain for sensorless induction motor drives in the wide-speed range," *IEEE Trans. Ind. Electron.*, vol. 70, no. 11, pp. 11055–11066, Nov. 2023, doi: 10.1109/TIE.2022.3227272.

[11] G. Sun, Z. Ma, and J. Yu, "Discrete-Time fractional order terminal sliding mode tracking control for linear motor," *IEEE Trans. Ind. Electron.*, vol. 65, no. 4, pp. 3386–3394, Apr. 2018.

[12] A. K. Junejo, W. Xu, C. Mu, M. M. Ismail, and Y. Liu, "Adaptive speed control of PMSM drive system based a new sliding-mode reaching law," *IEEE Trans. Power Electron.*, vol. 35, no. 11, pp. 12110–12121, Nov. 2020.

[13] B. Wang, Z. Dong, Y. Yu, G. Wang, and D. Xu, "Static-Errorless deadbeat predictive current control using second-order sliding-mode disturbance observer for induction machine drives," *IEEE Trans. Power Electron.*, vol. 33, no. 3, pp. 2395–2403, Mar. 2018.

[14] M. Morawiec and A. Lewicki, "Application of sliding switching functions in backstepping based speed observer of induction machine," *IEEE Trans. Ind. Electron.*, vol. 67, no. 7, pp. 5843–5853, Jul. 2020.

[15] B. Xu, L. Zhang, and W. Ji, "Improved non-singular fast terminal sliding mode control with disturbance observer for PMSM drives," *IEEE Trans. Transp. Electrific.*, vol. 7, no. 4, pp. 2753–2762, Dec. 2021.

[16] Y. Feng, X. Yu, and F. Han, "High-Order terminal sliding-mode observer for parameter estimation of a permanent-magnet synchronous motor," *IEEE Trans. Ind. Electron.*, vol. 60, no. 10, pp. 4272–4280, Oct. 2013.

[17] L. Gou, M. Zhou, and X. You, "Integral sliding mode control for starting speed sensorless controlled induction motor in the rotating condition," *IEEE Trans. Power Electron.*, vol. 35, no. 4, pp. 4105–4116, Apr. 2020.

[18] Y. Zhang, Z. Yin, Y. Zhang, J. Liu, and X. Tong, "A novel sliding mode observer with optimized constant rate reaching law for sensorless control of induction motor," *IEEE Trans. Ind. Electron.*, vol. 67, no. 7, pp. 5867–5878, Jul. 2020.

[19] J. Chen, X. Yuan, F. Blaabjerg, and C. H. T. Lee, "Overview of fundamental frequency sensorless algorithms for AC motors: A unified perspective," *IEEE J. Emerg. Sel. Topics Power Electron.*, vol. 11, no. 1, pp. 915–931, Feb. 2023.

[20] A. V. R. Teja, C. Chakraborty, and B. C. Pal, "Disturbance rejection analysis and FPGA-Based implementation of a second-order sliding mode controller fed induction motor drive," *IEEE Trans. Energy Convers.*, vol. 33, no. 3, pp. 1453–1462, Sep. 2018.

[21] C. Lascu, A. Argeseanu, and F. Blaabjerg, "Supertwisting sliding-mode direct torque and flux control of induction machine drives," *IEEE Trans. Power Electron.*, vol. 35, no. 5, pp. 5057–5065, May 2020.

[22] J. Mishra, L. Wang, Y. Zhu, X. Yu, and M. Jalili, "A novel mixed cascade finite-time switching control design for induction motor," *IEEE Trans. Ind. Electron.*, vol. 66, no. 2, pp. 1172–1181, Feb. 2019.

[23] Y. Feng, F. Han, and X. Yu, "Chattering free full-order sliding-mode control," *Automatica*, vol. 50, no. 4, pp. 1310–1314, 2014.

[24] M. Zhou, S. Cheng, Y. Feng, W. Xu, L. Wang, and W. Cai, "Full-Order terminal sliding-mode-based sensorless control of induction motor with gain adaptation," *IEEE J. Emerg. Sel. Topics Power Electron.*, vol. 10, no. 2, pp. 1978–1991, Apr. 2022.

[25] T. Wang, B. Wang, Y. Yu, and D. Xu, "Discrete sliding-mode-based MRAS for speed-sensorless induction motor drives in the high-speed range," *IEEE Trans. Power Electron.*, vol. 38, no. 5, pp. 5777–5790, May 2023.

[26] C. Zhang, "Robust fault-tolerant predictive current control for permanent magnet synchronous motors considering demagnetization fault," *IEEE Trans. Ind. Electron.*, vol. 65, no. 7, pp. 5324–5334, Jul. 2018.

Tianqing Wang was born in Heilongjiang Province, China, in 1997. He received the B.S. and M.S. degrees in electrical engineering in 2019 and 2021, respectively, from Harbin Institute of Technology (HIT), Harbin, China, where he is currently working toward Ph.D. degree in power electronics and electrical drives with the School of Electrical Engineering and Automation.

His research interests include sliding-mode control, and sensorless induction motor drives.

Bo Wang (Member, IEEE) was born in Shandong Province, China, in 1987. He received the B.S. degree in electrical engineering from Northwestern Polytechnical University, Xi'an, China, in 2011, and the M.S. and the Ph.D. degrees in electrical engineering from Harbin Institute of Technology (HIT), Harbin, China, in 2013 and 2017, respectively.

In 2017, he was with the School of Electrical Engineering and Automation, HIT, where he is currently an Associate Professor of electrical engineering. He has authored more than 30 technical papers published in journals and conference proceedings. His research interests include ac motor drives, sensorless control of ac motors, and nonlinear control theories.

Yong Yu was born in Jilin Province, China, in 1974. He received the B.S. degree in electromagnetic measurement and instrumentation, and the M.S. and the Ph.D. degrees in electrical engineering from Harbin Institute of Technology (HIT), Harbin, China, in 1995, 1997, and 2003, respectively.

From 2004 to 2014, he was an Associate Professor with the Department of Electrical Engineering, HIT, where he has been a Professor of Electrical Engineering since 2014. His current research interests include electrical motor drives, power quality mitigation, and fault diagnosis and tolerant control of inverter.

Dianguo Xu (Fellow, IEEE) received the B.S. degree in control engineering from Harbin Engineering University, Harbin, China, in 1982, and the M.S. and the Ph.D. degrees in electrical engineering from Harbin Institute of Technology (HIT), Harbin, China, in 1984 and 1989 respectively.

In 1984, he was with the Department of Electrical Engineering, HIT, as an Assistant Professor. Since 1994, he has been a Professor with the Department of Electrical Engineering, HIT. He was the Dean of School of Electrical Engineering and Automation, HIT, from 2000 to 2010. He was the Vice President of HIT from 2014 to 2020. His research interests include renewable energy generation technology, power quality mitigation, sensorless vector-controlled motor drives, high performance PMSM servo system. He published more than 600 technical papers.

Dr. Xu is the co-EIC for IEEE TRANSACTIONS ON POWER ELECTRONICS, and an Associate Editor for IEEE TRANSACTIONS ON INDUSTRIAL ELECTRONICS. He is the Chairman of IEEE Harbin Section.